arXiv:1409.6081v1 [astro-ph.SR] 22 Sep 2014

A Long-period Eccentric Substellar Companion to the Evovled Intermediate-Mass Star HD 14067

Liang Wang[1] Bun'ei Sato[2] Masashi Omiya[2] Hiroki Harakawa[2] Yujuan Liu[1] Nan Song[1,3] Wei He[1,3] Xiaoshu Wu[1,3] Hideyuki Izumiura[4,5] Eiji Kambe[4] Yoichi Takeda[5,6] Michitoshi Yoshida[7] Yoichi Itoh[8] Hiroyasu Ando[6] Eiichiro Kokubo[6] Shigeru Ida[2] and Gang Zhao[1]

[1] *Key Laboratory of Optical Astronomy, National Astronomical Observatories, Chinese Academy of Sciences, 20, Datun Road, Chaoyang District, Beijing 100012, China*

gzhao@nao.cas.cn

[2] *Tokyo Institute of Technology, 2-12-1 Ookayama, Meguro-ku, Tokyo 152-8550, Japan*

[3] *University of Chinese Academy of Sciences, 19A Yuquan Road, Shijingshan District, 100049 Beijing, China*

[4] *Okayama Astrophysical Observatory, National Astronomical Observatory of Japan, Kamogata, Okayama 719-0232, Japan*

[5] *The Graduate University for Advanced Studies, Shonan Village, Hayama, Kanagawa 240-0193, Japan*

[6] *National Astronomical Observatory of Japan, 2-21-1 Osawa, Mitaka, Tokyo 181-8588, Japan*

[7] *Hiroshima Astrophysical Science Center, Hiroshima University, Higashi-Hiroshima, Hiroshima 739-8526, Japan*

[8] *Nishi-Harima Astronomical Observatory, Center for Astronomy, University of Hyogo, 407-2, Nishigaichi, Sayo, Hyogo 679-5313, Japan*

(Received ; accepted)

Abstract

We report the detection of a substellar companion orbiting an evolved intermediate-mass ($M_\star = 2.4\,M_\odot$) star HD 14067 (G9 III) using precise Doppler technique. Radial velocities of this star can be well fitted either by a periodic Keplerian variation with a decreasing linear velocity trend ($P = 1455$ days, $K_1 = 92.2$ m s^{-1}, $e = 0.533$, and $\dot{\gamma} = -22.4$ m s^{-1} yr^{-1}) or a single Keplerian orbit without linear trend ($P = 2850$ days, $K_1 = 100.1$ m s^{-1}, and $e = 0.697$). The minimum mass ($m_2 \sin i = 7.8\,M_{\rm J}$ for the model with a linear trend, or $m_2 \sin i = 9.0\,M_{\rm J}$ for the model without a linear trend) suggests a long-period giant planet around an evolved intermediate-mass star. The eccentricity of the orbit is among the highest known for planets ever detected around evolved stars.

Key words: stars: individual (HD 14067) — stars: planetary systems — techniques: radial velocities

1. Introduction

Since the first giant planet orbiting evolved star was discovered by Frink et al. (2002), progress has been made on the detection and theoretical understanding of planet around stars more massive than our Sun in the past decade. Over 90 substellar companions with minimum masses ranging from 0.6 to 40 $M_{\rm J}$ around giants and subgiants have been detected by precise radial velocity technique (e.g. Sato et al. 2003; Setiawan et al. 2003; Hatzes et al. 2005; Johnson et al. 2007; Sato et al. 2008b; Döllinger et al. 2009; Liu et al. 2009; Wittenmyer et al. 2011; Johnson et al. 2011; Omiya et al. 2012; Gettel et al. 2012; Lee et al. 2013), including those in open clusters (e.g. Sato et al. 2007; Lovis & Mayor 2007; Brucalassi et al. 2014), in multiple-planet systems (e.g. Niedzielski et al. 2009; Sato et al. 2013b), and with masses $\gtrsim 13\,M_{\rm J}$ and thus lie in the brown dwarf regime (e.g. Omiya et al. 2009; Sato et al. 2010; Wang et al. 2012).

Although the number of such companions around GK giants is still insufficient to make a statistical study of their physical properties, they are of intense interest because their host stars are the slowly rotating counterparts of intermediate-mass ($1.5 < M_\star/M_\odot < 5$) B-A dwarfs that have evolved off the main sequence, giving us a chance to study planets orbiting stars with masses larger than those of FGK dwarfs. Recent studies have revealed some distinct differences from the FGK main sequence stars. For instance, nearly all detected planets around $M_\star > 1.5\,M_\odot$ stars have semi-major axes $\gtrsim 0.6$ AU, with only a few exceptions including HD 102956 b (Johnson et al. 2010), WASP-33 b (Collier Cameron et al. 2010), and Kepler-13 Ab (Szabó et al. 2011). Such paucity can be attributed to the engulfment by the host stars as they evolved off the main-sequence (Sato et al. 2008a; Nordhaus et al. 2010), or the primordial deficiency of short-period planets during their formations (e.g. Currie 2009; Kretke et al. 2009). On the other hand, most planets ever detected around intermediate-mass stars have eccentricities bellow 0.4. It is natural because most of their hosts are in the post-RGB (core helium burning) phase, and the planetary orbits could have been tidally circularized due to the increasing radii of the host stars as it ascends the red giant branch. However, some planets with high eccentricities ($e > 0.6$) have been discovered (e.g. Sato et al. 2013a; Moutou et al. 2011; Niedzielski et al. 2009), implying the existence of planet-planet scattering scenario (e.g. Ford & Rasio 2008) or perturbators (e.g. Takeda & Rasio 2005).

In this paper, we report on the detection of a new substellar companion around an intermediate-mass giant HD 14067 from our planet search program using the Subaru 8.2m telescope, the OAO 1.88m telescope and the Xinglong 2.16m telescope. Observations are described in section 2 and stellar properties are summarized in section 3. The analyses of radial velocities and orbital solutions are given in section 4. In section 5 we give the conclusion.

2. Observations and Radial-Velocity Analysis

We have been conducting a precise radial velocity survey for about 300 G-K giants at Okayama Astrophysical Observatory (OAO) Japan since 2001. To extend this planet search program, we established an international network among Japanese, Korean, and Chinese researchers using three 2m class telescopes in 2005 (East-Asian Planet Search Network; Izumiura 2005), and started the Subaru planet search program in 2006. By taking advantage of the large aperture (8.2m) of the Subaru Telescope, the planet-hosting candidates among a sample of ∼300 giants are quickly identified, and the visual magnitudes of $6.5 \leq V \leq 7.0$ enable them to be subsequently followed up by 2m class telescopes. For the details of the Subaru planet search program, readers are referred to the description by Sato et al. (2010).

We obtained a total of 3 spectra for HD 14067 in 2007 September, 2008 January and August using the High Dispersion Spectrograph (HDS; Noguchi et al. 2002) equipped with the Subaru Telescope. An iodine (I_2) absorption cell was used to provide a fiducial wavelength reference for precise radial velocity measurements (Kambe et al. 2002; Sato et al. 2002). We adopted the setup of StdI2b in the first two runs and StdI2a in the third one, which covered a wavelength region of 3500-6200 Å and 4900-7600 Å, respectively. The slit width was set to $0''.6$, giving a resolving power ($\lambda/\Delta\lambda$) of 60,000. The typical signal-to-noise ratio (S/N) was 140–200 pixel^{-1} with an exposure time of 30–50s.

After the observations at the Subaru Telescope, we started the follow-up observations using the 1.88m telescope with the High Dispersion Echelle Spectrograph (HIDES; Izumiura 1999) at OAO. The wavelength region was set to simultaneously cover 3750-7500 Å using the RED cross-disperser with a mosaic of three CCDs. We set the slit width to 200 μm ($0''.76$), giving a resolving power ($\lambda/\Delta\lambda$) of 67,000 with 3.3 pixel sampling, and used an iodine cell for precise wavelength calibration. We collected a total of 27 data points of HD 14067 with HIDES from October, 2008 to January, 2014.

Since November 2012, we started the follow-up observations of HD 14067 with the High Resolution Spectrograph (HRS) attached at the Cassegrain focus of the 2.16m telescope at Xinglong Observatory, China. The fiber-fed spectrograph is the successor of the Coudé Echelle Spectrograph (CES; Zhao & Li 2001), giving higher wavelength resolution and optical throughput. The single 4K × 4K CCD covers a wavelength region of 3700-9200 Å. The slit width was set to 190 μm, corresponding to a resolving power ($\lambda/\Delta\lambda$) of 45,000 with 3.2 pixel sampling. An iodine cell was installed before the fiber entrance to obtain the precise wavelength reference.

The reduction of the echelle spectra was performed using the IRAF [1] software package in the standard manner. The I_2-superposed spectra are modeled based on the algorithm given

[1] IRAF is distributed by the National Optical Astronomical Observatory, which is operated by the Association of Universities for Research in Astronomy, Inc., under cooperative agreement with the National Science Foundation.

by Sato et al. (2002, 2012). The stellar template used for radial velocity analysis was extracted by deconvolving an instrumental profile, which was determined from a spectrum of a B-star taken through the I_2 cell (Sato et al. 2012).

3. Stellar Properties

HD 14067 (HIP 10657, BD +23 307, HR 665, TYC 1765-1369-1) is listed in the Hipparcos Catalogue (Perryman et al. 1997) as a G9 III star, with a visual magnitude of $V = 6.53$ and a color index of $B - V = 1.025$. Its Hipparcos parallax $\pi = 6.12 \pm 0.79$ mas (van Leeuwen 2007) corresponds to a distance of 163.4 ± 12.3 pc and an absolute magnitude of $M_V = 0.33$. The effective temperature $T_{\rm eff} = 4815 \pm 100$ K and bolometric correction $BC = -0.329$ were derived from the color index $B - V$ and the estimated metallicity using the empirical calibration of Alonso et al. (1999, 2001). The color excess $E(B - V)$ was calibrated according to the reddening estimation given by Schlegel et al. (1998), and the interstellar extinction was found to be $A_V = 0.13$. The surface gravity $\log g = 2.61 \pm 0.10$ was determined from the triangular parallax given by the new reduction of the Hipparcos Catalogue (van Leeuwen 2007). The iron abundance [Fe/H] was determined from the equivalent widths of ∼30 unblended Fe lines measured from an iodine-free stellar spectrum taken with HIDES, and the LTE model atmosphere adopted in this work were interpolated from the ODFNEW grid of ATLAS9 (Castelli & Kurucz 2004). The stellar mass, radius and age were estimated using a Bayesian approach similar to that of da Silva et al. (2006). We used the Geneva database (Lejeune & Schaerer 2001), which covers the phases from the main-sequence to the early asymptotic giant branch (EAGB) stages for stars with $2 \leq M/M_\odot \leq 5$, to interpolate an extensive grid of stellar evolutionary tracks, with $\Delta M = 0.05$ within $1.2 \leq M/M_\odot \leq 3.6$, Δ[Fe/H] = 0.02 within -0.4 ≤ [Fe/H] ≤ +0.3, and 500 interpolated points in each track, spanning the whole evolutionary history. For each data points, the likelihood functions of $\log L$, $T_{\rm eff}$, and [Fe/H] were calculated to match the observed values by assuming a Gaussian error for each parameter. To simplify the calculation, we adopted uniform prior probabilities of mass and [Fe/H], but weighted the probability of each model with its spanning age along its evolutionary track. The details of the method will be described in an upcoming paper by Wang et al. (2014). The probability distribution functions (PDFs) of the parameters yield $M = 2.4 \pm 0.2\,M_\odot$, $R = 12.4 \pm 1.1\,R_\odot$ and age $= 0.69 \pm 0.20$ Gyr, and the probability that the star has passed through the RGB tip and in core helium burning phase is ∼97%. In figure 1, we plotted the HD 14067 on H-R diagram, together with the evolutionary tracks from Lejeune & Schaerer (2001) of stars with different masses and metal content. The macro turbulence velocity was estimated with the empirical relations of Hekker & Meléndez (2007) and the stellar rotational velocity $v \sin i$ is less than 1 km s^{-1} according to de Medeiros & Mayor (1999). We also determined the lithium abundance by fitting the line profile of Li I λ 6707.8 Å doublet using the spectra synthesis method with the IDL/SIU package. The results of $\log A(\mathrm{Li})_{\rm LTE} = 0.53$ and $\log A(\mathrm{Li})_{\rm NLTE} = 0.73$ suggest HD 14067

is a Li-depleted giant (Liu et al. 2014). The derived stellar parameters of HD 14067 are listed in table 1. Furthermore, the star shows no significant emission in the core of Ca II HK lines, as shown in figure 2, which suggests that HD 14067 is chromospherically inactive.

4. Radial Velocities and Orbital Solutions

We obtained a total of 52 velocity data points (27 from OAO, 22 from Xinglong, and 3 from Subaru) of HD 14067 over a span of more than 5 years. The radial velocities are listed in table 3 together with their estimated uncertainties. The generalized Lomb-Scargle periodogram (Zechmeister & Kürster 2009) of HD 14067 shows a significant peak with FAP (false-alarm probability) $< 1 \times 10^{-6}$ near the frequency of 4.9×10^{-4} c d^{-1} (figure 3). We also noticed that the star seems to exhibit a descendent linear velocity trend besides the periodic variability. The significance of the trend depends on how large systematic error is included in the first three Subaru data points, but it is difficult to be estimated. Therefore, we performed the least-squared orbital fitting by a single Keplerian with and without a linear trend, simultaneously. The orbital parameters and the uncertainties were derived using the Bayesian Markov Chain Monte Carlo (MCMC) method (e.g., Ford 2005; Gregory 2005; Ford & Gregory 2007), following the analysis in Sato et al. (2013a). We took account of velocity offsets of Xinglong and Subaru data relative to OAO data, $\Delta\mathrm{RV}_{\mathrm{Xinglong-OAO}}$ and $\Delta\mathrm{RV}_{\mathrm{Subaru-OAO}}$, as free parameters in the orbital fitting. Extra Gaussian noises for each of the three data sets, s_{OAO}, s_{Xinglong} and s_{Subaru}, including intrinsic stellar jitter as well as unknown noise source were also incorporated as free parameters. We generated 5 independent chains having 10^7 points with acceptance rate of about 25%, the first 10% of which were discarded, and confirmed each parameter was sufficiently converged based on the Gelman-Rubbin statistic (Gelman & Rubin 1992). We derived the median value of the merged posterior probability distribution function (PDF) for each parameter and set 1σ uncertainty as the range between 15.87% and 84.13% of the PDF.

In figure 5 we plot the best-fit Keplerian orbit with a linear velocity trend, together with the measured data points and their uncertainties obtained with the 3 different telescopes. The Keplerian orbit with a linear trend has parameters of period $P = 1455^{+13}_{-12}$ days, velocity semiamplitude $K_1 = 92.2^{+4.8}_{-4.7}$ m s^{-1}, eccentricity $e = 0.533^{+0.043}_{-0.047}$ and linear velocity trend $\dot{\gamma} = -22.4 \pm 2.2$ m s^{-1} yr^{-1}. Adopting the stellar mass of $M_\star = 2.4 \pm 0.2\,M_\odot$ given in table 1, we obtain $m_2 \sin i = 7.8 \pm 0.7\,M_{\mathrm{J}}$ and $a = 3.4 \pm 0.1$ AU for the companion. The R.M.S. scatter of the residuals to the Keplerian fit is 12.7 m s^{-1}. The Keplerian orbit without linear trend model yields the parameters of $P = 2850^{+430}_{-290}$ days, $K_1 = 100.1^{+4.9}_{-4.8}$ m s^{-1}, and $e = 0.697^{+0.045}_{-0.051}$, and the corresponding parameters of the companion are $m_2 \sin i = 9.0 \pm 0.9\,M_{\mathrm{J}}$ and $a = 5.3^{+0.6}_{-0.4}$ AU. The R.M.S. scatter of the residuals of this model is 14.3 m s^{-1}, and these solutions are also shown in figure 5. Since the R.M.S scatters of residuals in two models are close to each other and both are comparable to the radial velocity jitter ($\sim$8 m s^{-1}) due to the stellar oscillations estimated using the scaling relations of Kjeldsen & Bedding (1995), it is difficult to determine whether

the linear velocity trend should be included. We calculated the Bayesian information criterion ($\mathrm{BIC} = -2\ln\mathcal{L}_{\max} + k\ln N$; Schwarz 1978; Liddle 2004, 2007) of the two models, where $\mathcal{L}_{\max}$ is the maximum likelihood of each model, k denotes the number of free parameters in a model, and N is the number of data points. The Keplerian orbit with a linear velocity trend has smaller BIC value than the model without trend, but the former solution is largely constrained by the only 3 measurements with Subaru, and hence severely affected by the velocity offsets between data sets with different instruments. The velocity trend correspond to a possible outer companion with

$$\frac{m_{\rm c}\sin i_{\rm c}}{a_{\rm c}^2} \sim \frac{\dot{\gamma}}{G} = (0.13 \pm 0.01)\, M_{\rm J}\,{\rm AU}^{-2}$$

using the order-of-magnitude relation of Winn et al. (2009), where $m_{\rm c}$, $i_{\rm c}$ and $a_{\rm c}$ are mass, orbital inclination, and semi-major axis of the companion, respectively. This means if the companion lies outside $\sim$ 10 AU, it shall not be an exoplanet with $m_{\rm c} < M_{\rm b}$, where $M_{\rm b} \simeq 13\,M_{\rm J}$ is the lower mass limit of a typical brown dwarf. On the other hand, there is no evidence that HD 14067 has any companion star so far. After removal of the orbital fitting, there is no significant peak with FAP$>$ 0.1 on the generalized Lomb-Scargle periodograms of the velocity residuals (figure 4).

The Hipparcos satellite made a total number of 86 photometric observations for HD 14067 during the period from Jan. 1990 to Feb. 1993. The scatter of $\mathrm{H_p}$ magnitude is down to 0.007 mag, but the photometry is not contemporaneous with the radial velocity measurements and also the time span ($\sim$1100 days) is not long enough to cover a whole radial velocity period. Figure 6 shows the generalized Lomb-Scargle periodogram of the HD 14067 photometric data. We did not find any clue that the radial velocity variation correlates with the brightness changes due to the stellar spots.

We also performed spectral line shape analysis for the star following the method in Sato et al. (2007). Cross correlation profiles of the two stellar templates, which were extracted from five $\mathrm{I_2}$-superposed spectra at phases of velocity maximum (JD$\sim$2455600) and minimum (JD$\sim$2455900) using the technique by Sato et al. (2002), were derived for about 90 spectral segments (4–5Å width each). Then three bisector quantities of the cross correlation profiles, BVS, BVC, and BVD, were calculated, which are the velocity difference between the two flux level of the bisector, the difference of the BVS of the upper and lower half of the bisector, and the average of the bisector at three flux levels, respectively. We used the flux levels of 25, 50, and 75% of each cross correlation profile to calculate the above three bisector quantities. As a result, we obtained BVS$= -8.4 \pm 3.8\,{\rm m\,s^{-1}}$, BVC$= 2.7 \pm 1.8\,{\rm m\,s^{-1}}$, and BVD$= -186.7 \pm 7.1\,{\rm m\,s^{-1}}$ ($\simeq 2K_1$), suggesting that the observed radial velocity variations are not caused by distortion of the spectral lines but by parallel shifts of them as expected in the case of orbital motion.

5. Conclusion

We report the detection of a long-period substellar companion to the G9 III evolved intermediate-mass ($M = 2.4\,M_{\odot}$) star HD 14067 from the Subaru and Japan-China planet search program. The radial velocity variation of the star can be best explained by the gravitational perturbation of an unseen surrounding companion. The orbit can be well fitted with two models - a Keplerian orbit with and without a linear velocity trend, both of which have similar velocity residuals, while the former model has smaller BIC value than the latter one. The minimum mass of the companion is $m_2 \sin i = 7.8 \pm 0.7\,M_{\rm J}$ (with velocity trend) or $m_2 \sin i = 9.0 \pm 0.9\,M_{\rm J}$ (without trend), suggesting a long-period giant planet orbiting around an evolved giant star. It is notable that HD 14067 b is among the planets with the largest semi-major axes and orbital periods around evolved intermediate-mass stars. The possible decreasing linear velocity trend ($-22.4\,{\rm m\,s^{-1}\,yr^{-1}}$) may suggests an additional outer companion around this star. Unfortunately, the time span of observations is not long enough neither to distinguish between these two possible orbital solutions nor to confirm the existence of this outer companion. Therefore, the continued radial velocity observations are essential to characterize the orbital properties of this system.

Although the fitting of Keplerian orbit with a linear trend significantly reduce the resulting eccentricity, orbital solutions with both models show the eccentricity of the HD 14067 b is large ($e = 0.533$ with a velocity trend, or $e = 0.697$ without velocity trend), making this planet one of the most eccentric ones ever discovered around stars with $M_{\star} > 1.5\,M_{\odot}$. Figure 8 shows a concentration towards low eccentricity for planets around off-main sequence stars ($\log g_{\star} < 3.5$), while the eccentricity distribution of planets around main sequence stars reach its peak at $e = 0.2 \sim 0.3$. To avoid the bias due to the lack of short-period, circularized planets around evolved stars, only planets with semi-major axes 0.5 AU $< a <$ 3.0 AU are plotted. The high eccentricity of HD 14067 b might originate from (a) the incomplete circularization due to its large distance to its host, because $|\dot{e}|$ decreases as a^{-8} (Zahn 1989), or (b) the perturbation of an outer companion. We plot the eccentricities against the semi-major axes of exoplanets found around evolved and main sequence stars with Doppler technique in figure 7, where the colors are coded with different ranges of stellar mass. It is clearly shown that almost all planets orbiting high-mass ($M_{\star} > 2.0\,M_{\odot}$) stars have periastron distances [$q = a(1-e)$] > 0.66 AU. The closest blue point to HD 14067 b in figure 7 is HD 120084 b, which also has an eccentric orbit ($a = 4.3$ AU, $e = 0.66$, see Sato et al. 2013a) around an evolved star with $M_{*} = 2.39\,M_{\odot}$. The large semi-major axes of these two long-period planets support the former possibility of the origin of the large eccentricities, which means they were less affected by the orbital circularization during the RGB phase compared with other planets around evolved stars. We also noticed most planet-harboring evolved stars accompanied by eccentric planets ($e > 0.4$) also exhibit linear radial velocity trends besides the periodic variations caused by their companions,

or lie in systems with more than two objects. For example, HD 1690 (with an eccentric planet of $e = 0.64 \pm 0.04$) shows a linear decreasing velocity trend of $\dot{\gamma} = -7.2 \pm 0.4\,\mathrm{m\,s^{-1}}$ (Moutou et al. 2011). HD 102272 c ($e = 0.68 \pm 0.06$) is the outer companion of a double-planet system (Niedzielski et al. 2009). And the parent stars of HD 137759 b ($e = 0.70 \pm 0.01$, Frink et al. 2002) and HD 110014 b ($e = 0.462 \pm 0.069$, de Medeiros et al. 2009) are both members of double star systems. These facts imply that the high eccentricities of such planets can be excited by the gravitational perturbations of additional objects, or the existences of these objects stop the orbital circularizations of the planets. If the relatively small eccentricities of planets around evolved stars are caused by the tidal circularization when the parent stars expand during the RGB phase, it is expected to see higher orbital eccentricities with increasing semi-major axes, especially in the systems where a distant outer perturbator exists. Future discoveries with longer observational baseline will be of great help to answer this crucial question.

This research is based on data collected at the Subaru Telescope, and Okayama Astrophysical Observatory (OAO), both operated by National Astronomical Observatory of Japan (NAOJ), and the 2.16m telescope at Xinglong Observatory, operated by National Astronomical Observatories, Chinese Academy of Sciences. We are grateful to all the staff members of Subaru, OAO, and Xinglong for their support during the observations. We thank students of Tokyo Institute of Technology and Kobe University for their kind help for the observations at Subaru and OAO. LW is supported by the Young Researcher Grant of National Astronomical Observatories, Chinese Academy of Sciences. BS was partly supported by MEXT's program "Promotion of Environmental Improvement for Independence of Young Researchers" under the Special Coordination Funds for Promoting Science and Technology and by Grant-in-Aid for Young Scientists (B) 20740101 from the Japan Society for the Promotion of Science (JSPS). BS is supported by Grant-In-Aid for Scientific Research (C) 23540263 from JSPS and HI is supported by Grant-In-Aid for Scientific Research (A) 23244038 from JSPS. YJL and LW are supported by the National Natural Science Foundation of China under grants 11173031. This research has made use of the SIMBAD database, operated at CDS, Strassbourg, France.

References

Alonso, A., Arribas, S., & Martínez-Roger, C. 1999, A&AS, 140, 261
Alonso, A., Arribas, S., & Martínez-Roger, C. 2001, A&A, 376, 1039
Brucalassi, A., Pasquini, L., Saglia, R., et al. 2014, A&A, 561, L9
Castelli, F. & Kurucz, R. L. 2004, ArXiv Astrophysics e-prints
Collier Cameron, A., Guenther, E., Smalley, B., et al. 2010, MNRAS, 407, 507
Currie, T. 2009, ApJL, 694, L171
da Silva, L., Girardi, L., Pasquini, L., et al. 2006, A&A, 458, 609

de Medeiros, J. R. & Mayor, M. 1999, A&AS, 139, 433
de Medeiros, J. R., Setiawan, J., Hatzes, A. P., et al. 2009, A&A, 504, 617
Döllinger, M. P., Hatzes, A. P., Pasquini, L., et al. 2009, A&A, 499, 935
Ford, E. B. 2005, AJ, 129, 1706
Ford, E. B. & Gregory, P. C. 2007, in Astronomical Society of the Pacific Conference Series, Vol. 371, Statistical Challenges in Modern Astronomy IV, ed. G. J. Babu & E. D. Feigelson, 189
Ford, E. B. & Rasio, F. A. 2008, ApJ, 686, 621
Frink, S., Mitchell, D. S., Quirrenbach, A., et al. 2002, ApJ, 576, 478
Gelman, A. & Rubin, D. 1992, Statistical Science, 7, 457
Gettel, S., Wolszczan, A., Niedzielski, A., et al. 2012, ApJ, 745, 28
Gregory, P. C. 2005, ApJ, 631, 1198
Hatzes, A. P., Guenther, E. W., Endl, M., et al. 2005, A&A, 437, 743
Hekker, S. & Meléndez, J. 2007, A&A, 475, 1003
Horne, J. H. & Baliunas, S. L. 1986, ApJ, 302, 757
Izumiura, H. 1999, Publications of the Yunnan Observatory, 77
Izumiura, H. 2005, Journal of Korean Astronomical Society, 38, 81
Johnson, J. A., Bowler, B. P., Howard, A. W., et al. 2010, ApJL, 721, L153
Johnson, J. A., Clanton, C., Howard, A. W., et al. 2011, ApJS, 197, 26
Johnson, J. A., Fischer, D. A., Marcy, G. W., et al. 2007, ApJ, 665, 785
Kambe, E., Sato, B., Takeda, Y., et al. 2002, PASJ, 54, 865
Kjeldsen, H. & Bedding, T. R. 1995, A&A, 293, 87
Kretke, K. A., Lin, D. N. C., Garaud, P., & Turner, N. J. 2009, ApJ, 690, 407
Lee, B.-C., Han, I., & Park, M.-G. 2013, A&A, 549, A2
Lejeune, T. & Schaerer, D. 2001, A&A, 366, 538
Liddle, A. R. 2004, MNRAS, 351, L49
Liddle, A. R. 2007, MNRAS, 377, L74
Liu, Y.-J., Sato, B., Zhao, G., & Ando, H. 2009, Research in Astronomy and Astrophysics, 9, 1
Liu, Y. J., Tan, K. F., Wang, L., et al. 2014, ApJ, 785, 94
Lovis, C. & Mayor, M. 2007, A&A, 472, 657
Moutou, C., Mayor, M., Lo Curto, G., et al. 2011, A&A, 527, A63
Niedzielski, A., Goździewski, K., Wolszczan, A., et al. 2009, ApJ, 693, 276
Noguchi, K., Aoki, W., Kawanomoto, S., et al. 2002, PASJ, 54, 855
Nordhaus, J., Spiegel, D. S., Ibgui, L., Goodman, J., & Burrows, A. 2010, MNRAS, 408, 631
Omiya, M., Han, I., Izumioura, H., et al. 2012, PASJ, 64, 34
Omiya, M., Izumiura, H., Han, I., et al. 2009, PASJ, 61, 825
Perryman, M. A. C., Lindegren, L., Kovalevsky, J., et al. 1997, A&A, 323, L49

Sato, B., Ando, H., Kambe, E., et al. 2003, ApJL, 597, L157
Sato, B., Izumiura, H., Toyota, E., et al. 2008a, PASJ, 60, 539
Sato, B., Izumiura, H., Toyota, E., et al. 2007, ApJ, 661, 527
Sato, B., Kambe, E., Takeda, Y., Izumiura, H., & Ando, H. 2002, PASJ, 54, 873
Sato, B., Omiya, M., Harakawa, H., et al. 2012, PASJ, 64, 135
Sato, B., Omiya, M., Harakawa, H., et al. 2013a, PASJ, 65, 85
Sato, B., Omiya, M., Liu, Y., et al. 2010, PASJ, 62, 1063
Sato, B., Omiya, M., Wittenmyer, R. A., et al. 2013b, ApJ, 762, 9
Sato, B., Toyota, E., Omiya, M., et al. 2008b, PASJ, 60, 1317
Schlegel, D. J., Finkbeiner, D. P., & Davis, M. 1998, ApJ, 500, 525
Schwarz, G. 1978, The Annals of Statistics, 6, 461
Setiawan, J., Hatzes, A. P., von der Lühe, O., et al. 2003, A&A, 398, L19
Szabó, G. M., Szabó, R., Benkő, J. M., et al. 2011, ApJL, 736, L4
Takeda, G. & Rasio, F. A. 2005, ApJ, 627, 1001
van Leeuwen, F. 2007, A&A, 474, 653
Wang, L., Sato, B., Wu, X. S., Liu, Y. J., & Zhao, G. 2014, in preparation
Wang, L., Sato, B., Zhao, G., et al. 2012, Research in Astronomy and Astrophysics, 12, 84
Winn, J. N., Johnson, J. A., Albrecht, S., et al. 2009, ApJL, 703, L99
Wittenmyer, R. A., Endl, M., Wang, L., et al. 2011, ApJ, 743, 184
Zahn, J.-P. 1989, A&A, 220, 112
Zechmeister, M. & Kürster, M. 2009, A&A, 496, 577
Zhao, G. & Li, H.-B. 2001, Chinese J. Astron. Astrophys., 1, 555

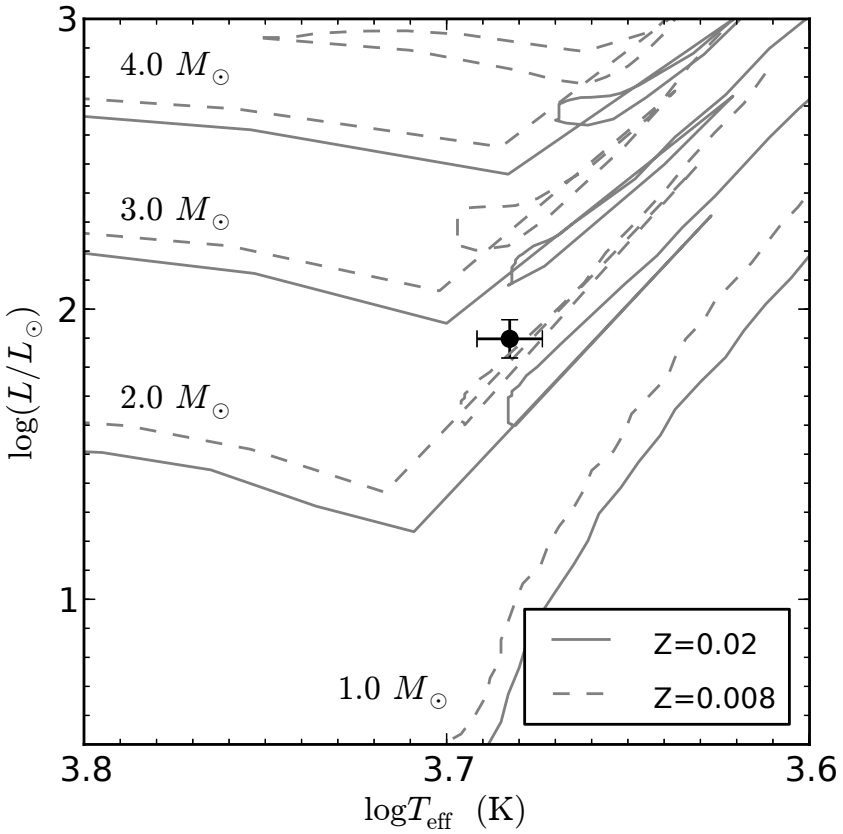

Fig. 1. H-R diagram. The solid cricle represents HD 14067, with the errorbars corresponding to the uncertainties given in table 1. The solid and dashed lines reprensent the evolution tracks from Lejeune & Schaerer (2001) for stars of $M = 1 \sim 4\,M_\odot$ with $Z = 0.02$ (solar metallicity) and $Z = 0.008$, respectively.

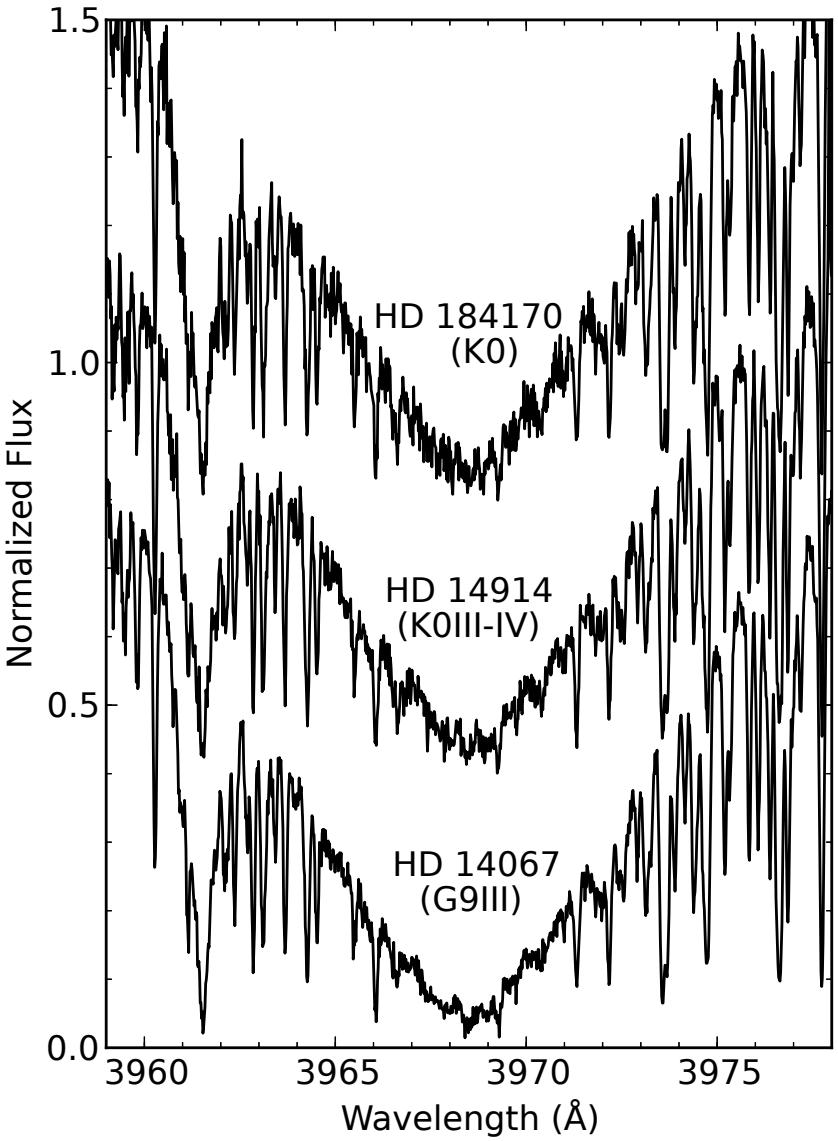

Fig. 2. Spectra in the region of Ca H lines. Stars with similar spectral type to HD 14067 are also shown in this figure. A vertical offset of 0.4 is added to each spectrum.

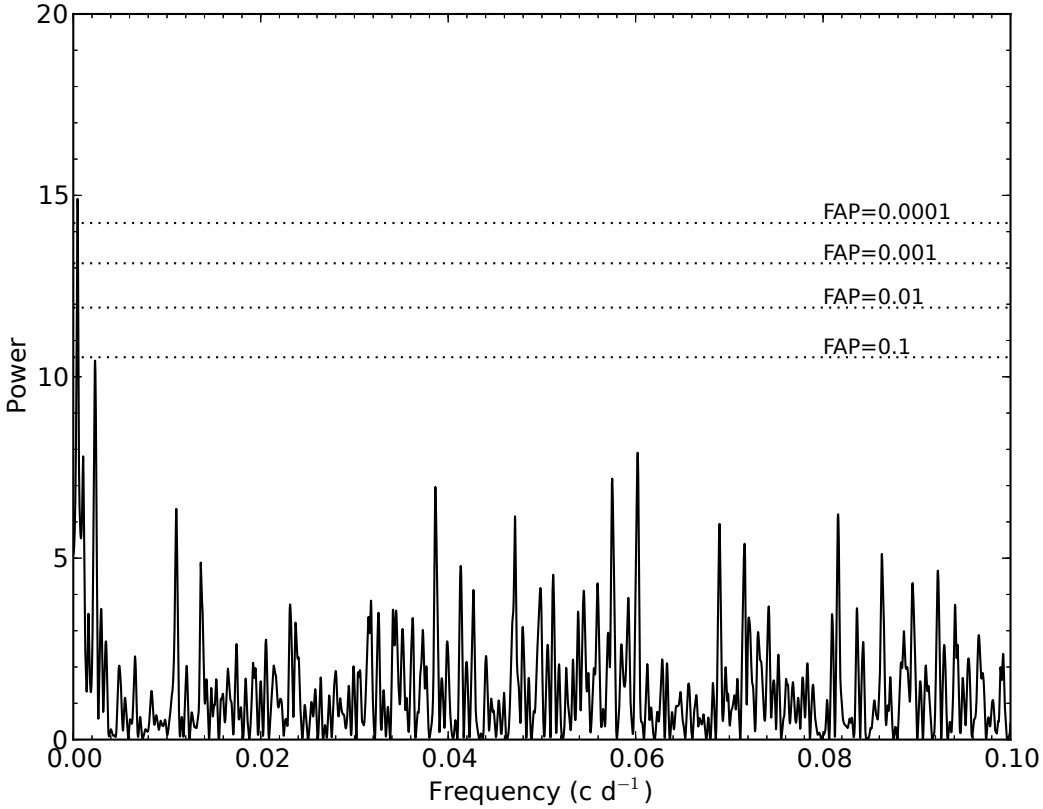

Fig. 3. Generalized Lomb-Scargle periodogram of the radial velocities of HD 14067. The normalization and FAP (false-alarm probability) were calculated according to Horne & Baliunas (1986). There is a significant peak at $f \sim 4.9 \times 10^{-4}\,\mathrm{c\,d^{-1}}$, with the FAP $< 1 \times 10^{-6}$. The dash horizontal lines indicate the FAP levels of 10^{-1}, 10^{-2}, 10^{-3}, and 10^{-4}, respectively, from the bottom to the top.

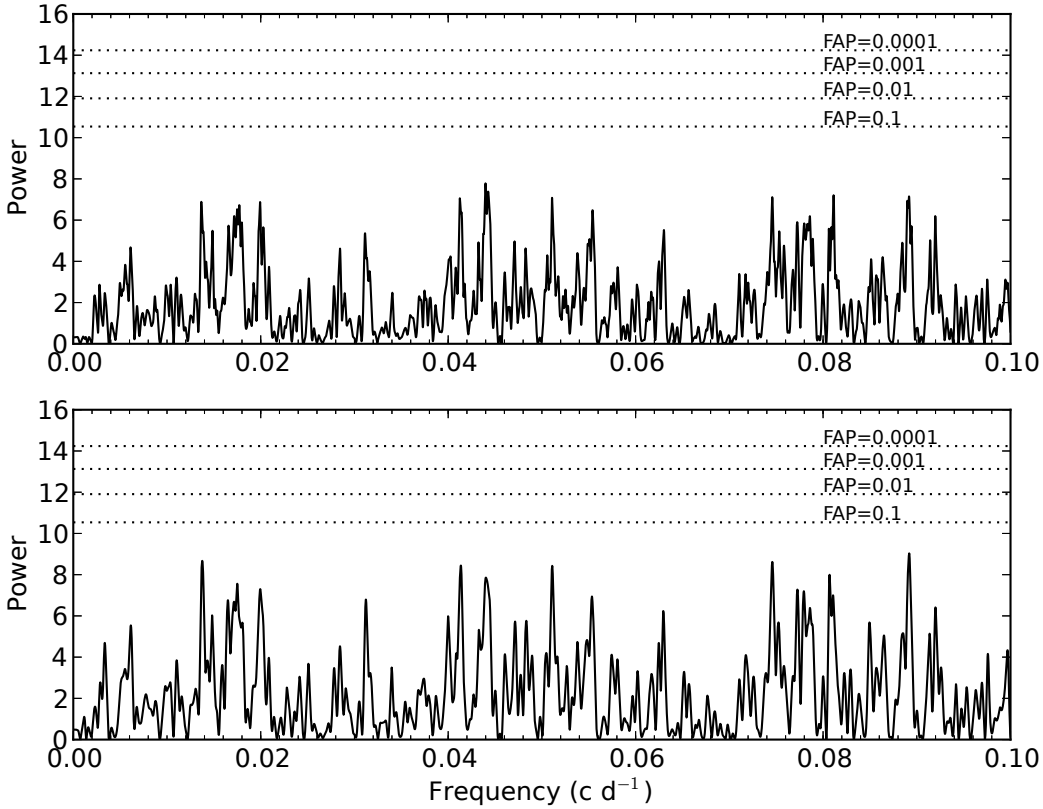

Fig. 4. Generalized Lomb-Scargle periodograms of the radial velocity residuals after Keplerian orbital fitting with (*upper panel*) and without (*lower panel*) a linear trend. Neither of them shows any significant peak with FAP above 0.1.

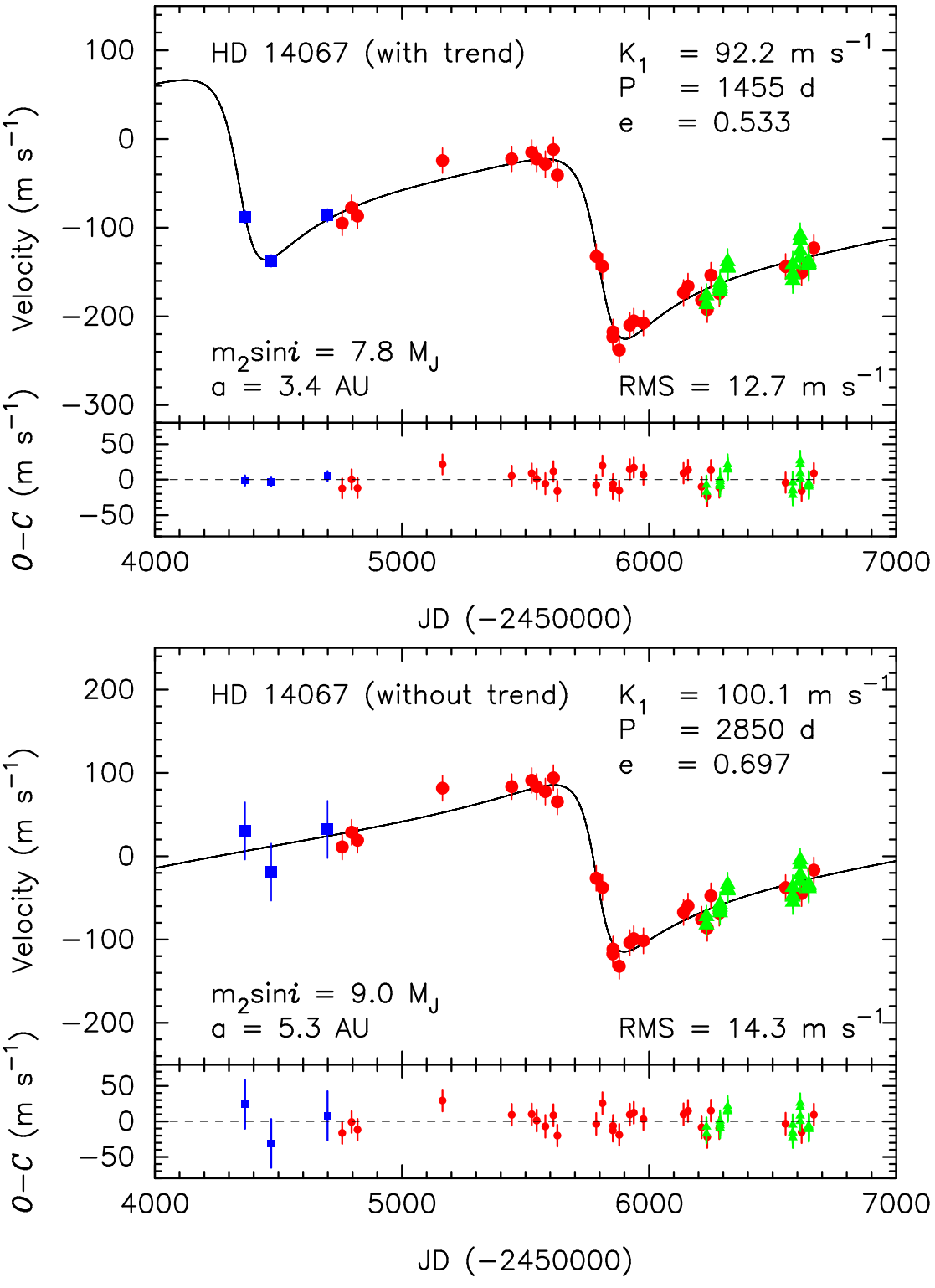

Fig. 5. Radial velocities of HD 14067 observed at OAO (red circles), Xinglong (green triangles), and Subaru (blue squares). The error bar for each point includes the stellar jitter. The Keplerian orbits with (*top panel*) and without (*bottom panel*) a linear velocity trend are shown by the solid lines. Residuals to the orbit fits are also shown in each panel. The R.M.S. is 12.7 m s^{-1} (with linear trend) and 14.3 m s^{-1} (without linear trend), respectively.

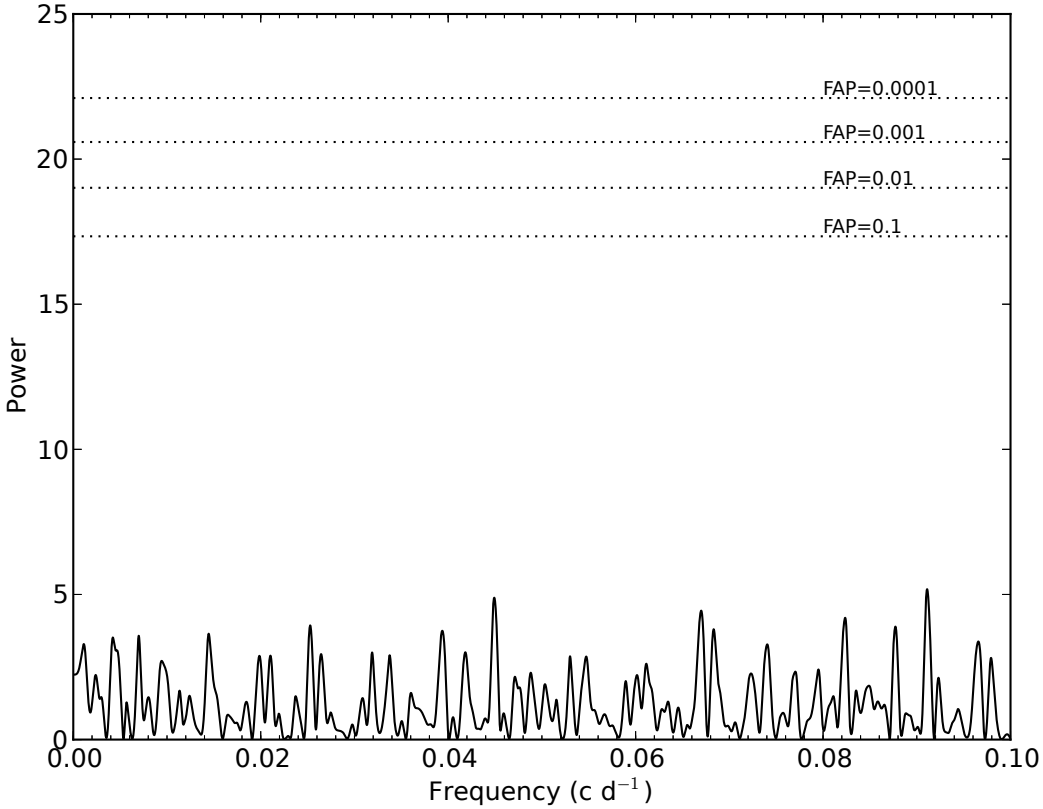

Fig. 6. Generalized Lomb-Scargle periodogram of the Hipparcos photometric data of HD 14067. The dash horizontal lines indicate the FAP levels of 10^{-1}, 10^{-2}, 10^{-3}, and 10^{-4}, respectively, from the bottom to the top.

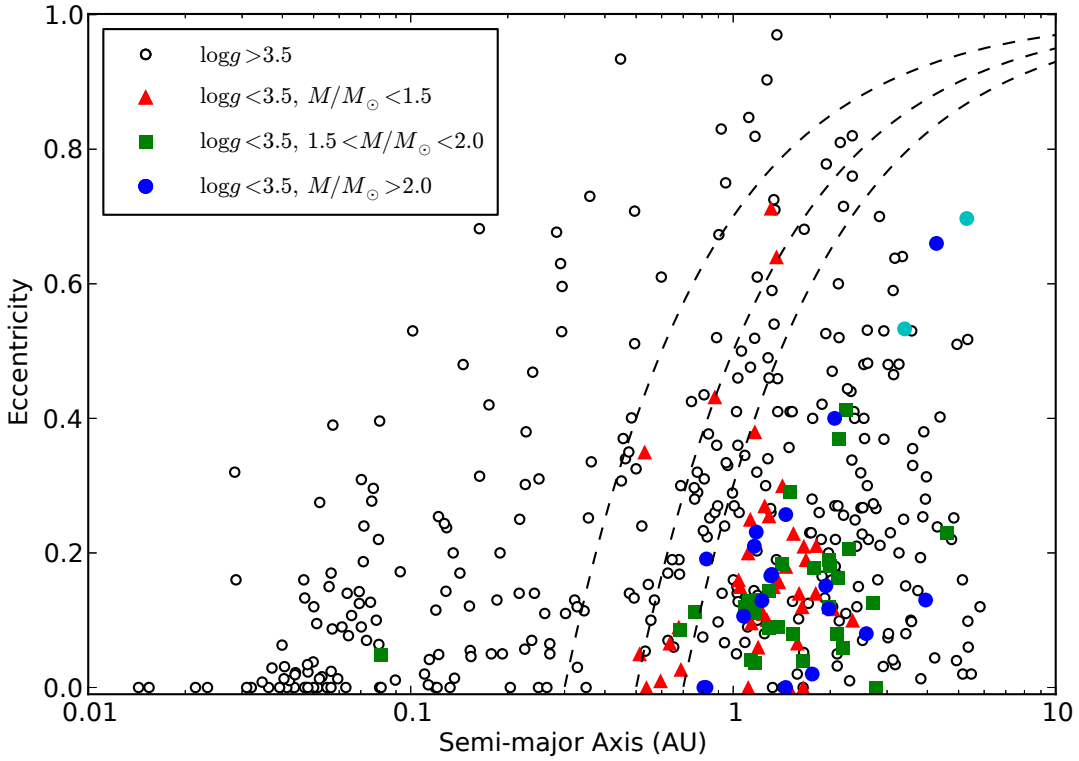

Fig. 7. Eccentricities versus semi-major axes of exoplanets discovered by radial velocity technique. Planets around low-mass ($M_\star < 1.5\,M_\odot$), intermediate-mass ($1.5\,M_\odot < M_\star < 2.0\,M_\odot$), and high-mass ($M_\star > 2.0\,M_\odot$) evolved stars with $\log g_\star < 3.5$ are plotted by red filled triangles, green filled squares, and blue filled circles, respectively. The two possible solutions of the newly detected companion HD 14067 b is plotted by the cyan circles. Planets around stars with $\log g_\star > 3.5$ are plotted by open circles. Dashed lines indicate the periastron distance [$q = a(1-e)$] of 0.3, 0.5, and 0.7 AU, respectively, from the left to the right.

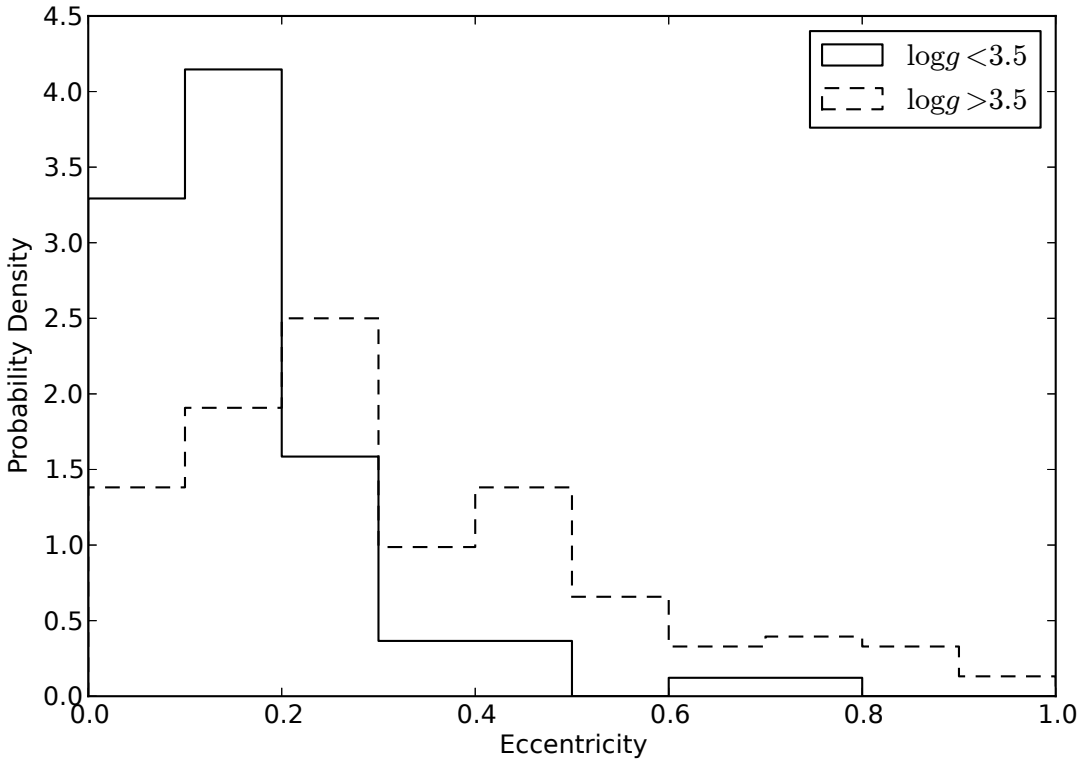

Fig. 8. Probability density distribution of eccentricities of radial velocity planets with 0.5 AU $< a <$ 3.0 AU around main sequence stars ($\log g_\star > 3.5$), and around evolved stars ($\log g_\star < 3.5$) are plotted by dashed lines and solid lines, respectively.

Table 1. Stellar parameters of HD 14067

Parameter	HD 14067
Sp. type	G9 III
π (mas)	6.12 ± 0.46
Distance (pc)	163.4 ± 12.3
V	6.53
$B-V$	1.025
A_V	0.14
M_V	0.33
BC	-0.329
$T_{\rm eff}$ (K)	4815 ± 100
$\log g$	2.61 ± 0.10
[Fe/H]	-0.10 ± 0.08
$v_{\rm t}$ ($\rm km\,s^{-1}$)	1.30 ± 0.15
L ($L_\odot$)	79 ± 12
R ($R_\odot$)	12.4 ± 1.1
M ($M_\odot$)	2.4 ± 0.2
age (Gyr)	0.69 ± 0.20
$v_{\rm macro}$ ($\rm km\,s^{-1}$)	5.44 ± 0.45
$v \sin i$ ($\rm km\,s^{-1}$)	< 1 (de Medeiros & Mayor 1999)
$\log A$(Li)	0.53 (LTE), 0.73 (NLTE)

Table 2. Orbital parameters of HD 14067 b

Parameter	HD 14067 b	
	with trend	without trend
P (days)	1455^{+13}_{-12}	2850^{+430}_{-290}
K_1 ($\mathrm{m\,s^{-1}}$)	$92.2^{+4.8}_{-4.7}$	$100.1^{+4.9}_{-4.8}$
e	$0.533^{+0.043}_{-0.047}$	$0.697^{+0.045}_{-0.051}$
ω (deg)	$109.9^{+5.6}_{-5.7}$	$102.1^{+5.1}_{-5.3}$
T_p (JD−2,450,000)	1443^{+31}_{-37}	92^{+586}_{-862}
s_OAO ($\mathrm{m\,s^{-1}}$)	$13.8^{+2.6}_{-2.0}$	$14.9^{+2.7}_{-2.1}$
s_Xinglong ($\mathrm{m\,s^{-1}}$)	$12.2^{+3.0}_{-2.4}$	$12.3^{+3.0}_{-2.4}$
s_Subaru ($\mathrm{m\,s^{-1}}$)	$5.4^{+22.2}_{-4.6}$	34^{+31}_{-14}
$\Delta\mathrm{RV}_\mathrm{Xinglong-OAO}$ ($\mathrm{m\,s^{-1}}$)	$19.8^{+6.0}_{-6.0}$	$21.5^{+6.1}_{-6.2}$
$\Delta\mathrm{RV}_\mathrm{Subaru-OAO}$ ($\mathrm{m\,s^{-1}}$)	$3.6^{+11.3}_{-12.5}$	$-8.7^{+24.1}_{-24.2}$
$\dot{\gamma}$ ($\mathrm{m\,s^{-1}\,yr^{-1}}$)	$-22.4^{+2.2}_{-2.2}$	–
$a_1 \sin i$ (10^{-3} AU)	$10.43^{+0.50}_{-0.51}$	$18.9^{+1.8}_{-1.4}$
$f_1(m)$ ($10^{-7}\,M_\odot$)	$0.714^{+0.099}_{-0.91}$	$1.10^{+0.16}_{-0.15}$
$m_2 \sin i$ (M_J)	7.8 ± 0.7	9.0 ± 0.9
a (AU)	3.4 ± 0.1	$5.3^{+0.6}_{-0.4}$
N_OAO	27	
N_Xinglong	22	
N_Subaru	3	
RMS ($\mathrm{m\,s^{-1}}$)	12.7	14.3
BIC	447.07	458.24

Table 3. Radial Velocities of HD 14067

JD (−2450000)	Radial Velocity ($m\,s^{-1}$)	Uncertainty ($m\,s^{-1}$)	Observatory
4758.11638	33.7	3.2	OAO
4796.20144	51.3	3.3	OAO
4820.01616	41.8	3.0	OAO
5164.16162	104.3	3.5	OAO
5444.14944	106.1	3.2	OAO
5525.16330	113.6	3.2	OAO
5545.11627	106.2	4.0	OAO
5580.00227	100.2	5.7	OAO
5612.94961	116.7	4.5	OAO
5628.91329	87.9	3.8	OAO
5786.27403	−3.9	3.5	OAO
5811.19593	−15.1	3.9	OAO
5853.23042	−94.8	5.1	OAO
5854.22657	−88.9	3.5	OAO
5879.18379	−109.5	3.8	OAO
5922.00916	−81.2	3.8	OAO
5938.00117	−76.6	3.8	OAO
5976.91135	−79.0	3.5	OAO
6139.23229	−44.8	4.5	OAO
6157.28469	−37.3	3.8	OAO
6212.29616	−53.1	3.8	OAO
6235.19638	−63.7	4.4	OAO
6250.20981	−25.0	3.6	OAO
6284.05633	−45.7	4.0	OAO
6552.26042	−15.2	4.1	OAO
6617.07400	−22.2	3.7	OAO
6666.87938	5.8	4.6	OAO
6232.11546	−38.1	5.3	Xinglong
6232.13878	−28.3	5.1	Xinglong
6286.95306	−13.5	8.1	Xinglong
6286.97627	−16.9	7.9	Xinglong
6287.00037	−20.3	7.4	Xinglong
6287.02420	−23.6	7.7	Xinglong
6317.94617	10.1	7.8	Xinglong

Table 3. (Continued.)

JD (−2450000)	Radial Velocity ($m\,s^{-1}$)	Uncertainty ($m\,s^{-1}$)	Observatory
6317.96965	3.4	7.6	Xinglong
6317.99284	2.8	7.9	Xinglong
6318.01605	4.8	8.6	Xinglong
6581.18750	6.8	8.3	Xinglong
6581.21073	−3.7	6.7	Xinglong
6581.23392	−4.8	8.0	Xinglong
6581.25725	−10.9	8.2	Xinglong
6611.11370	14.2	6.9	Xinglong
6611.13689	21.9	7.4	Xinglong
6611.16007	34.2	7.4	Xinglong
6611.18325	39.9	6.4	Xinglong
6646.03568	8.9	12.1	Xinglong
6646.05898	10.6	11.6	Xinglong
6646.08226	7.1	13.3	Xinglong
6646.10544	5.4	12.5	Xinglong
4364.95416	44.2	4.8	Subaru
4470.70735	−5.2	4.1	Subaru
4698.90077	46.0	5.0	Subaru